IEEE Access
Multidisciplinary | Rapid Review | Open Access Journal

Received December 20, 2017, accepted January 22, 2018, date of publication February 6, 2018,
date of current version September 28, 2018.

Digital Object Identifier 10.1109/ACCESS.2018.2801564

Optimal Component Sizing of a Four-Wheel Independently-Actuated Electric Vehicle With a Real-Time Torque Distribution Strategy

ZHENPO WANG, CHANGHUI QU, LEI ZHANG, (Member, IEEE), XUE XUE, AND JIANYANG WU
National Engineering Laboratory for Electric Vehicles, Beijing Institute of Technology, Beijing 100081, China
Collaborative Innovation Center of Electric Vehicles in Beijing, Beijing Institute of Technology, Beijing 100081, China

Corresponding author: Lei Zhang (lei_zhang@bit.edu.cn)

This work was supported in part by the Ministry of Science and Technology, China, under Grant 2017YFB0103600, and in part by the Beijing Municipal Science and Technology Commission under Grant B160603.

ABSTRACT This paper investigates the optimal component sizing problem for a four-wheel-independently-actuated electric vehicle. First, a real-time optimal distribution strategy is devised to allocate the torque demands to each actuation motor of the vehicle with the aim to make them work in high-efficiency regions as often as possible. The primary goal is to minimize the energy consumption per hundred kilometers while maximizing the driving range per charge. Then, the particle swarm optimization (PSO) is employed to globally search for the optimal sizing solution, which is later verified by the Genetic algorithm. Simulation results show that the proposed PSO-based optimization method, combined with the real-time torque distribution strategy, can effectively downsize the main powertrain components and lead to better energy consumption.

INDEX TERMS Four-wheel-independently-actuated electric vehicle, optimal sizing, real-time torque distribution strategy, particle swarm optimization.

I. INTRODUCTION

Electric vehicles (EVs) have been ubiquitously considered as a promising means to deal with the dilemma of oil depletion and environmental pollution [1], [2]. EVs can make use of electricity stored in onboard energy storage devices for vehicle propulsion. The consumed electricity can be produced from renewable energy sources such as solar and wind energy and hydro-electric power. Recently, four-wheel-independently-actuated electric vehicles (FWIA EVs) have attracted tremendous interest from both industry and academia because of its actuation flexibility and potential for overall powertrain efficiency improvement [3]. Typically, four in-wheel motors are used yet independently controlled through the vehicle control unit (VCU) in a FWIA EV. These motors can generate different torques in a coordinated manner to generate an additional yaw-moment. This actuation flexibility has the potential to enhance the vehicle lateral stability and handling performance [4], [5]. Moreover, the overall powertrain efficiency can be further improved, owing to the elimination of mechanical transmission systems and the optimized operating regime of each motor [6], [7]. For example, only front-axle motors are designated to work near their high-efficiency zones on occasions where the totally required driving power is far below the sum of the rated power of motors, thus resulting in elevated powertrain efficiency.

There exists a rich library of literature that presents all-around studies on FWIA EVs, in which research on dynamic performance and powertrain efficiency improvements are the focuses. It is well acknowledged that these improvements are highly related to enabling torque allocation strategies, which has incurred considerable endeavors. Generally, torque allocation strategies can be grouped into two categories, i.e., the equal distribution strategy and the real-time torque distribution strategy. The former is actually a special form of real-time torque distribution strategy where the total torque requirement is evenly dispatched to the front- and rear-axle motors. It intuitively represents a scenario in which all the in-wheel motors work in a very similar condition and somehow can be regarded as a generic motor. This can serve as the benchmark to assess the performance of the real-time torque distribution strategy, which often makes the most of activation flexibility of FIAW EVs through

optimal torque distribution to each motor. For the later, the axial load transfer, tire slip rate limitations, and motor and inverter losses constitute the main concerns. For instance, Harada *et al.* proposed a model-based range extension control scheme for acceleration and deceleration scenarios, and developed a real-time torque distribution strategy considering tire slip ratio, copper loss and iron loss of motors [8]. Wang *et al.* [9] presented a torque distribution strategy for a front-and-rear-wheel-driven electric vehicle, which accounts for the weight transfer between front- and rear-axles and motor losses. Fujimoto and Harada [10] presented a method to address front and rear driving-braking forces distribution, which was proved to be effective in increasing the driving range of EVs in simulation and bench tests. Park *et al.* [11] developed an integrated torque distribution strategy taking into consideration of tire slip and vehicle cornering. Kim [12] investigated the optimal power distribution of the front and rear motors for minimizing energy consumption of a FWIA EV, and evaluated its performance by comparing the energy consumption to that with the simple power distribution control. Wang *et al.* [13] proposed a torque distribution algorithm to minimize the power consumption during the longitudinal motion. Lee *et al.* [14] proposed a method of regulating the switchings between two-wheel and four-wheel drives for FWIA EVs to realize overall efficiency optimization considering the losses of motors and inverters. Chen and Wang [15] put forward various energy-efficient control allocation strategies for FWIA EVs, and verified them in a set of driving conditions. The above mentioned studies mainly focused on improving overall system efficiency, but there is a lack of literature exploring the optimal component sizing problem for FWIA EVs.

In contrast, there exist a considerable number of research papers reporting on sizing for hybrid electric vehicles (HEVs), plug-in HEVs (PHEVs), and multi-energy source (fuel cell/battery/supercapacitor) EVs [16]–[18]. Both energy management strategies and advanced optimization algorithms need to be included for optimal component sizing. The commonly-used optimization methods include Particle Swarm Optimization (PSO), Genetic Algorithms (GAs) and Simulated Annealing (SA), and the like. For example, Dimitrova and Maréchal [19] presented a design methodology based on the GA method for HEVs. Li *et al.* [20] proposed a novel hybrid GA for the simultaneous optimization of the powertrain and control parameters for a plug-in electric bus considering both fuel economy and dynamic performance. Still, Chen *et al.* [21] presented a novel optimal power management approach for PHEVs against uncertain driving conditions. Similarly, the PSO algorithm was used to optimize the threshold parameters of a rule-based power management strategy under a certain driving cycle [22].

Similar to the GAs, PSO is a stochastic global optimization approach, which has the advantages of simplicity, easy implementation and requiring few parameters. Moreover, the aforementioned studies have revealed that PSO is a rapid and reliable tool for developing energy management strategies, and can always outperform other evolutionary algorithms [23]–[25].

The primary aim of this study is to analyze the co-relationship between vehicle dynamic performance and powertrain parameters. This is cast as an optimal component sizing problem, with emphasis on the influence of parameters variation. The main contributions of this study lie in the following aspects: (1) a component sizing optimization problem for a FWIA EV is formulated and solved by PSO, whose reliability is further verified by the GA algorithm; (2) under the prerequisite of vehicle performance preservation, the maximum driving range and the specific equivalent energy consumption are balanced through a multi-objective cost function under typical driving conditions.

The remainder of this paper is structured as follows: Section II presents the vehicle model for an FWIA EV. Section III formulates and derives the optimization problem. Section IV presents and discusses the main simulation results, followed by the key conclusions summarized in Section V.

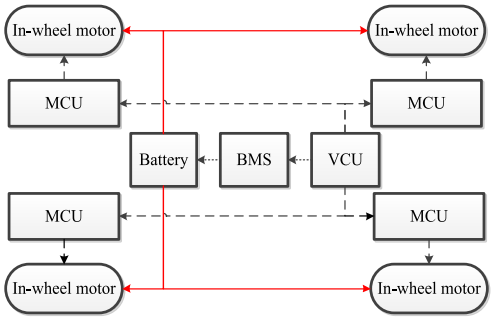

FIGURE 1. The configuration of the powertrain structure.

II. VEHICLE MODELING

The powertrain of the studied FWIA EV is mainly composed of four in-wheel motors, a DC\DC converter, an on-board charger, a vehicle control unit (VCU), four motor control units (MCUs) and a battery pack and battery management system (BMS). It is worth noting that the in-wheel motors are independently controlled by their respective MCUs. Since MCUs and BMS have much less energy consumption compared to the loss of motors, it is reasonable to ignore their influence on the overall power consumption in this study. The vehicle configuration is sketched in Figure 1 for demonstration.

The quasi-static system model is adopted here as shown in Figure 2. It includes a vehicle dynamics model, a generalized battery model, an in-wheel motor model and several target driving cycles. The vehicle is able to follow the dynamic profiles generated from a library of selected driving cycles. The model has a loop control structure, which calculates the required mechanical power to follow the target dynamic cycles. This control loop is termed as "back and forward", which allows for simulating the energy consumption on a

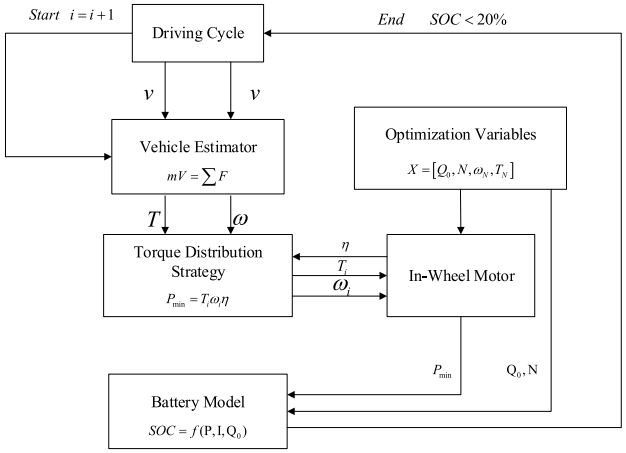

FIGURE 2. The system model of four-wheel independently actuated electric vehicle.

given driving profile, and the energy flow is computed backwards from the wheels to the energy source.

A. GENERALIZED BATTERY MODEL

In this study, a generalized lithium-ion battery model is adopted due to its simplicity and acceptable accuracy. The battery voltage during charging/discharging processes can be derived according to the Kirchhoff's current law as [26]

$$\begin{cases} U_b = U_{oc} - I_a R_{int} & \text{(Discharge)} \\ U_b = U_{oc} + I_a R_{int} & \text{(Charge)} \end{cases} \tag{1}$$

As illustrated in Figure. 2, the model input is the power demand and the output is the battery state-of-charge (SOC). Their functional relationship can be expressed as

$$\begin{cases} P_{bat} = U_b I_a \\ P_{bat} = U_{oc} I_a - I_a^2 R_{int} \end{cases} \tag{2}$$

The battery SOC is defined as the ratio of the delivered charge Q(t) over the nominal battery capacity Q_0 in Ah, which can be derived by

$$SOC_{end} = SOC_{ini} - \frac{\int_0^t I_a dt}{Q_0} \tag{3}$$

The total mass m_{bat} of the battery pack includes the weights of constituent battery cells and the associated enclosure. The specific energy of battery q_{batt} and the mass of enclosure m_{box} are approximately 80Wh/kg and 28kg, respectively. Then, the relationship between the total mass and the voltage and rated capacity of the battery pack can be derived as

$$m_{bat} = \frac{CU_0 N}{q_{batt}} + m_{box} \tag{4}$$

As shown in Figure 3, experiments have been conducted on lithium-ion phosphate ($LiFePO_4$) batteries with different capacities to analyze how the open circuit voltage(OCV) and the internal resistance change with battery SOC. Then, the surface fitting is applied to approximate the OCV and the internal resistance based on capacity and SOC values using the cubic polynomial functions as follows:

$$\begin{aligned} U_{oc} = & -2.73 \times SOC - 0.15 \times C - (4.32 \times SOC^2) \\ & - 0.002 \times C^2 \times 10^{-6} - 0.004 \times SOC \times C \\ & + 2.47 \times SOC^3 + 8.16 \times 10^{-6} C^3 - 1.06 \end{aligned} \tag{5}$$

$$\begin{aligned} R_{int} = & -0.08 \times SOC + 0.01 \times C + 0.07 \times SOC^2 \\ & - 0.0002 \times C^2 \times 10^{-6} + 0.0004 \times SOC \times C \\ & - 0.03 \times SOC^3 + 7.54 \times C^3 + 0.81 \end{aligned} \tag{6}$$

B. GENERALIZED IN-WHEEL MOTOR MODEL

The permanent magnet synchronous in-wheel motors [27] are utilized, and the mass of each motor can be approximated as

$$m_{motor} = a \times T_{max} + b \tag{7}$$

where a and b are the empirical fitting parameters. Normally, $a = 0.0567$ Kg/Nm and $b = 16.3$kg.

The calculation model proposed by Abdul-Hak [28] is applied here to calculating the motor efficiency. Once the maximum power of motor P_{max} (kW), the maximum torque of motor T_{max} (Nm), the maximum rotation rate ω_{max} (rad/s), the rated power T_N (Nm) and the rated voltage of battery pack U_{bat} are given, the motor efficiency can be determined based on the following assumptions:

(1) The Kulun torque and viscous friction account for 2% and 6% of all power losses of the motor under the maximum power corresponding to the maximum speed, and the motor achieves the highest efficiency at the point of rated operation. Accordingly, under the maximum output power of the motor, the motor achieves the maximum efficiency at the point of motor speed corresponding to the rated torque, which can be calculated as $\omega_{T_N} = P_{max}/T_N$.

(2) The motor efficiency working at its maximum power and maximum speed is known and defined as η_{pnmax}, the phase angle of voltage/current as Φ_N, the power factor of the motor corresponding to this phase angle as $cos\Phi_N$.

The Kulun torque and viscous friction can be calculated by

$$T_{coul} = 0.02 \frac{P_{\max}}{\omega_{\max} \eta_{Pn\max}} \tag{8}$$

$$B_{vis} = 0.06 \frac{P_{\max}}{\omega_{\max}^2 \eta_{Pn\max}} \tag{9}$$

The electromagnetic torque corresponding to the rated torque is defined as

$$T_{en} = T_{coul} + B_{vis} \omega_{T-N} + T_N \tag{10}$$

The motor is designed based on parameters including the motor speed corresponding to the rated torque, the maximum power, and the minimum bus voltage. The motor speed is approximately proportional to the terminal voltage. The motor is capable of outputting the maximum speed at the minimum bus voltage, and the value of the corresponding modulation parameter m_{imax} is 1. Therefore, if the motor is designed based on the rated torque, the modulation parameter

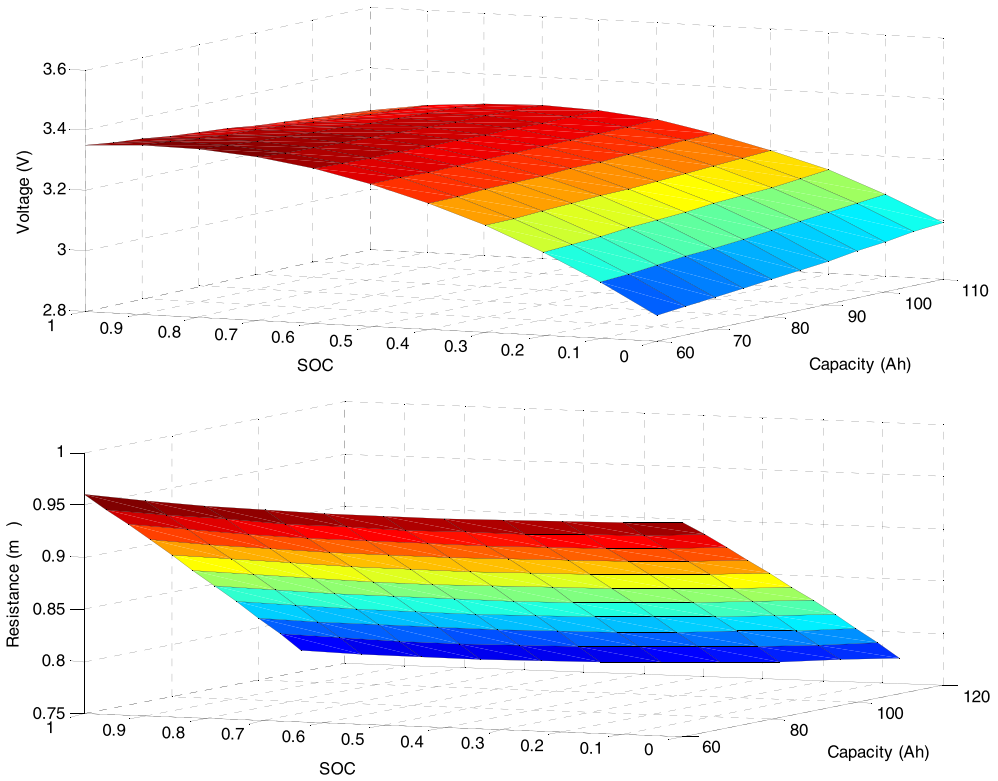

FIGURE 3. The relationship between the OCV and the internal resistance with different SOCs and capacities of batteries.

corresponding to the minimum supply voltage of the motor can be calculated as

$$m_{iN} = \frac{\omega_{T-N}}{\omega_{\max}} m_{i\max} \tag{11}$$

$$\widehat{U}_{PN} = m_{iN} \frac{U_{Bat,\min}}{2} \tag{12}$$

The voltage of d- and q-axis of the motor are given as

$$U_{dN} = -\widehat{U}_{PN} \sin f_N \tag{13}$$

$$U_{qN} = \widehat{U}_{PN} \cos \phi_N \tag{14}$$

The motor parameters are calculated by making magnetic field vector and current vector orthogonal as

$$L_q = -\frac{4U_{dN}P_{\max}}{3P\omega_{T_N}\eta_{m\max}} \tag{15}$$

$$R_s = \frac{3\left(PP_{\max}U_{qN}^2 - T_{eN}\omega_{eN}U_{qN}\eta_{m\max}\right)}{2PP_{\max}P_{m\max}} \tag{16}$$

Once the output torque and speed of the motor are given, its efficiency can be calculated by

$$i_q = \frac{T_{coul} + B_{vis}\omega + T}{3 \times \frac{P}{4}\lambda_m} \tag{17}$$

$$U_q = R_s i_q + \frac{P}{2}\lambda_m \omega \tag{18}$$

$$\eta_m = \frac{P}{P_m} = \frac{T\omega}{\frac{3}{2}U_q i_q} \tag{19}$$

C. TORQUE DISTRIBUTION STRATEGIES

1) EQUAL DISTRIBUTION STRATEGY

The total driving torque equates to the sum of torques generated by each actuation motor as given in Eq. (20). The torque allocation is equally designated to each motor under the equal distribution strategy as shown in Eq. (21). In this study, the steering motion is neglected so that the left and right motors output the same torque for both the front- and rear-axle wheels.

$$T_{total} = T_{front} + T_{rear} \tag{20}$$

$$T_i = \frac{F_{total}r}{4}, \quad i = 1, 2, 3, 4 \tag{21}$$

2) REAL-TIME OPTIMAL DISTRIBUTION STRATEGY

The torque demands distributed to the front-axle wheels are different from that to the rear-axle ones. The distributed torque demands are calculated with the principle of enhancing the overall powertrain efficiency, which is time-varying and strongly dependent on the driving cycles. Figure 4 shows the flow chart of the proposed real-time distribution strategy.

The driving torque of each wheel is defined in Eq. (22), assuming that the inertial torque is ignored. The k denotes the distribution coefficient. Particularly, $k = 0$ means the front-axle drive only while $k = 1$ means the rear-axle drive only.

$$T_i = F_i r = \begin{cases} \frac{r}{2}kF_{total}, & i = 1, 2 \\ \frac{r}{2}(1-k)F_{total}, & i = 3, 4 \end{cases} \tag{22}$$

where F_i represents the driving force of the i-th wheel.

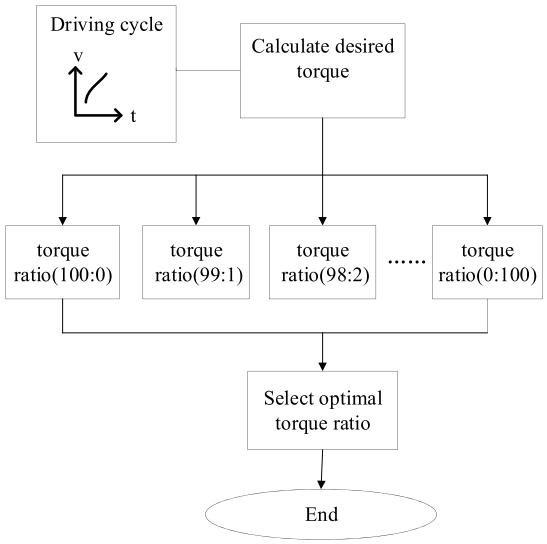

FIGURE 4. Flow chart of the real-time distribution strategy.

The constraint to each in-wheel motor is defined as

$$-T_{i_{\max}} \le T_i \le T_{i_{\max}} \tag{23}$$

For a single-wheel model, the slip ratio is given as

$$\lambda_i = \frac{\omega_i r - V_x}{\max(\omega_i r, V_x)} \tag{24}$$

where V_x, λ_i and ω_i are the vehicle velocity, tire slip ratio, and angular velocity of the wheel.

Moreover, the friction coefficient between the tire and road is a function of λ_i, and the driving force can be represented as

$$F_i = D_s \cdot N_i \cdot \lambda_i \tag{25}$$

For simplicity, the driving stiffness D_s is substituted into Eq. (26) by assuming a linear relationship between λ_i and μ_i as

$$D_s = \left.\frac{\partial \mu_i}{\partial \lambda_i}\right|_{\lambda_i=0} \tag{26}$$

The normal forces on the four wheels are

$$\begin{cases} N_1 = N_2 = \dfrac{m_{total} \cdot \left(l_r \cdot g - h_g \cdot \dot{V}_x\right)}{2l} \\ N_3 = N_4 = \dfrac{m_{total} \cdot \left(l_r \cdot g + h_g \cdot \dot{V}_x\right)}{2l} \end{cases} \tag{27}$$

$$m_{total} = m_{bat} + m_{motor} + m_{body} \tag{28}$$

The total driving/braking torque is calculated according to the real-time working conditions, and the efficiency is derived from the efficiency map, which is later used to estimate the actual power consumption. The wheel angular velocity of each wheel can be obtained as

$$\omega_i = \begin{cases} \dfrac{V_x}{r} \cdot \dfrac{1}{1-\lambda_i}, V_x \ge \omega_i r \\ \dfrac{V_x}{r}(1+\lambda_i), V_x \le \omega_i r \end{cases} \tag{29}$$

The total motor output P_{mot} can be deduced as

$$P_{mot} = \begin{cases} \dfrac{\sum_{i=1}^{2} T_i k \omega_i}{\eta_{front}} + \dfrac{\sum_{i=3}^{4} T_i (1-k)\omega_i}{\eta_{rear}} & \text{(Discharge)} \\ \eta_{front} \sum_{i=1}^{2} T_i k \omega_i & \\ \quad + \eta_{rear} \sum_{i=3}^{4} T_i (1-k)\omega_i & \text{(Charge)} \end{cases} \tag{30}$$

where η_{front} and η_{rear} represent the efficiencies of the front-axle and rear-axle motors, respectively. The motor efficiency depends on the working conditions including the motor torque and speed. In other words, the battery power can be conserved by improving the overall efficiency through regulating the working conditions of motors, which means to optimize the torque allocation to the front-axle and rear-axle motors. The discharging efficiency of the battery is assumed to be 95%, and thus the battery power can be calculated by $P_{bat} = P_{mot}/95\%$.

Thus, the consumed energy E_{veh} can further derived by

$$E_{veh} = \int P_{bat} dt \tag{31}$$

At each time index, the optimal distribution coefficient k can be determined by comparing the energy consumption under each k. Consequently, this real-time distribution strategy can save the stored energy to a great extent by increasing the driving efficiency through torque allocation optimization.

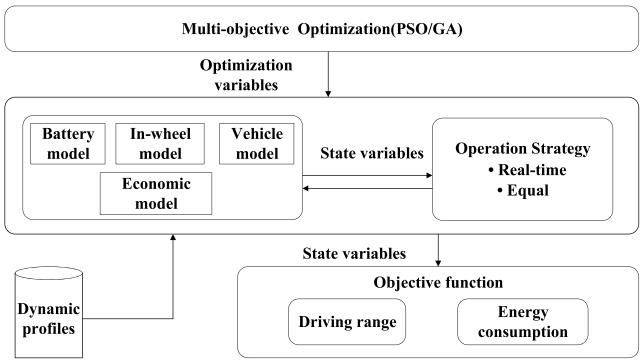

FIGURE 5. The schematic of the multi-objective optimization.

III. PARAMETERS OPTIMIZATION PROBLEM FORMULATION

The schematic of the proposed multi-objective optimization problem formulation is illustrated in Figure 5. The optimal component sizing is cast as an optimization problem, in which the optimization variables represent a possible combination of components sizing. In each iteration of PSO/GA algorithms, the equal and real-time torque distribution strategies are implemented respectively to evaluate the objective function under a specific driving cycle. This process is iterated until the termination conditions are fulfilled, and the best sizing is derived.

TABLE 1. Performance requirements.

Sequence number	Constraints	Description [a]
1	Grade-ability	≥20%,at 40km/h
2	Acceleration time,	Time for 0-100km/h≤15s
3	Maximum speed	≥120km/h
4	Driving range	≥150km
5	power consumption per hundred kilometers	≤18kWh

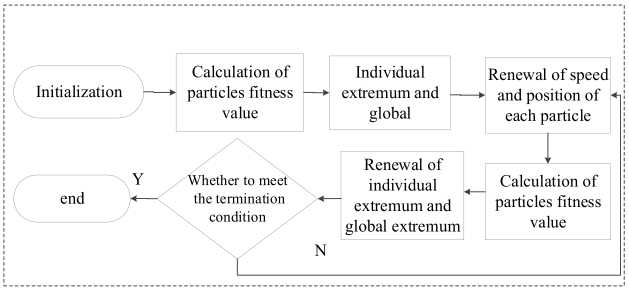

FIGURE 6. The flow-process diagram of the PSO algorithm.

A. THE OPTIMIZATION VARIABLES

The primary goal of component sizing is to minimize the power consumption per hundred kilometers and maximize the driving range without compromising the vehicle performance. However, these two aspects are conflicting. In this study, the optimal design is formulated as a multi-objective optimization problem by taking these two objectives into consideration. The battery cell capacity, the number of batteries, the rated rotatory speed and the rated torque of the motor are selected as the optimization variables, which are capsulated as

$$X = [Q_0, N, \omega_N, T_N] \tag{32}$$

B. OPTIMIZATION CONSTRAINTS

The vehicle performance requirements are incorporated into the optimization problem as the constraints, as listed in Table I.

C. OPTIMIZATION PROBLEM DESCRIPTION

The driving range calculation under the driving-cycle case is more complicated than that in the constant-speed case because vehicles would endure different driving modes including the constant speed, acceleration, deceleration and idle speed in a single driving cycle.

Considering the regenerative braking, the energy consumption of the vehicle in a driving cycle can be calculated as follows.

When the in-wheel motors are in the driving mode, the power in need can be deduced by

$$P_{cyc\_d} = \frac{V_x}{3600\eta_t\eta_m\eta_{ac}}\left(m_{total}gf + \frac{C_dAV_x^2}{21.15} + \delta m_{total}\dot{V}_x\right) \tag{33}$$

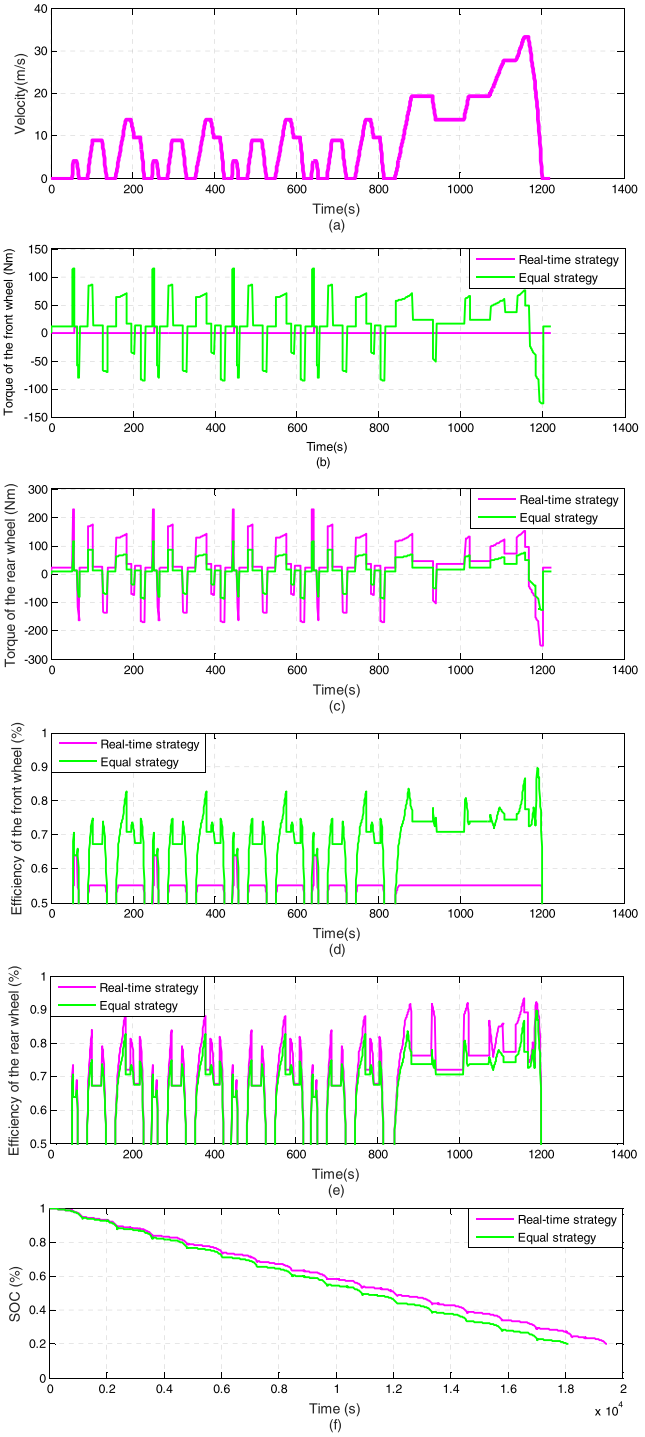

FIGURE 7. Simulation results with different distribution strategy. (a) NEDC speed profile; (b) Torque of the front wheels; (c) Torque of the rear wheels; (d) Efficiency of the front wheels; (e) Efficiency of the rear wheels (f) Battery SOC.

When the in-wheel motors are in the braking mode, the power in need can be obtained as

$$P_{cyc\_c} = \eta_t\eta_m\eta_{ac}\frac{V_x}{3600}\left(m_{total}gf + \frac{C_dAV_x^2}{21.15} + \delta m_{total}\dot{V}_x\right) \tag{34}$$

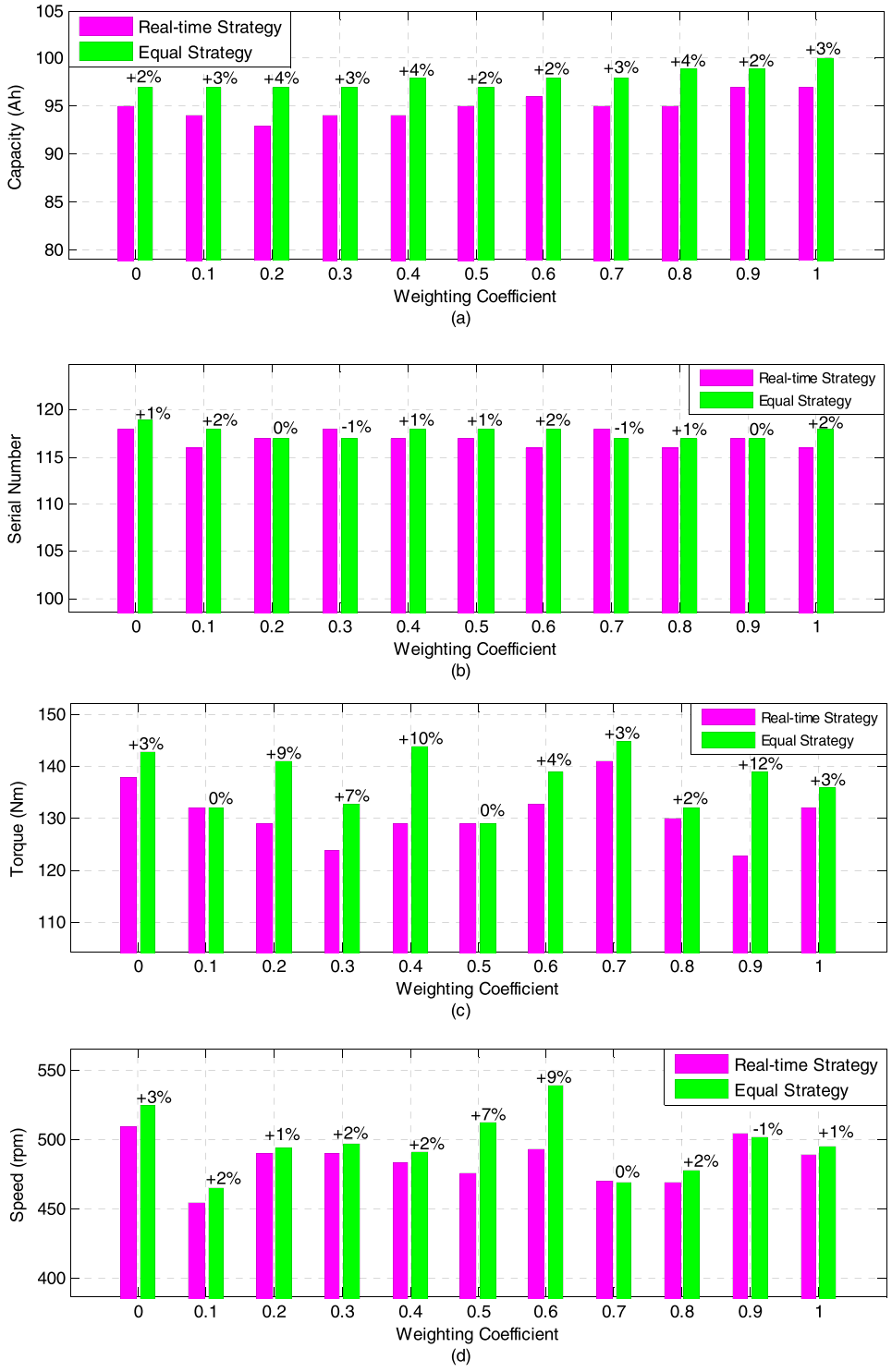

FIGURE 8. Selection of vehicle parameters for different torque distribution strategies.

The total energy consumption in the whole driving cycle can be calculated by

$$w_{cyc} = \frac{100}{S_{cyc}} \left(\int_0^{T_{cyc}} \frac{P_{cyc\_d}}{\eta_{b\_d}} dt + \int_0^{T_{cyc}} P_{cyc\_c} \eta_{b\_c} dt \right) \quad (35)$$

With the goal-attainment method, the multi-objective optimization problem can be converted into a single-objective problem as follows:

$$\begin{cases} \cos t_{\_func} = \omega_1 \lambda_1 / \ s(X) + \omega_2 \lambda_2 w_{\text{cyc}}(X) & (X \subset \Omega) \\ \lambda_1 \geq 0, \quad \lambda_2 \geq 0 \\ \lambda_1 + \lambda_2 = 1 \end{cases} \quad (36)$$

where $s(X)$ and $w_{cyc}(X)$ represent the driving range per charge and the power consumption per hundred kilometers,

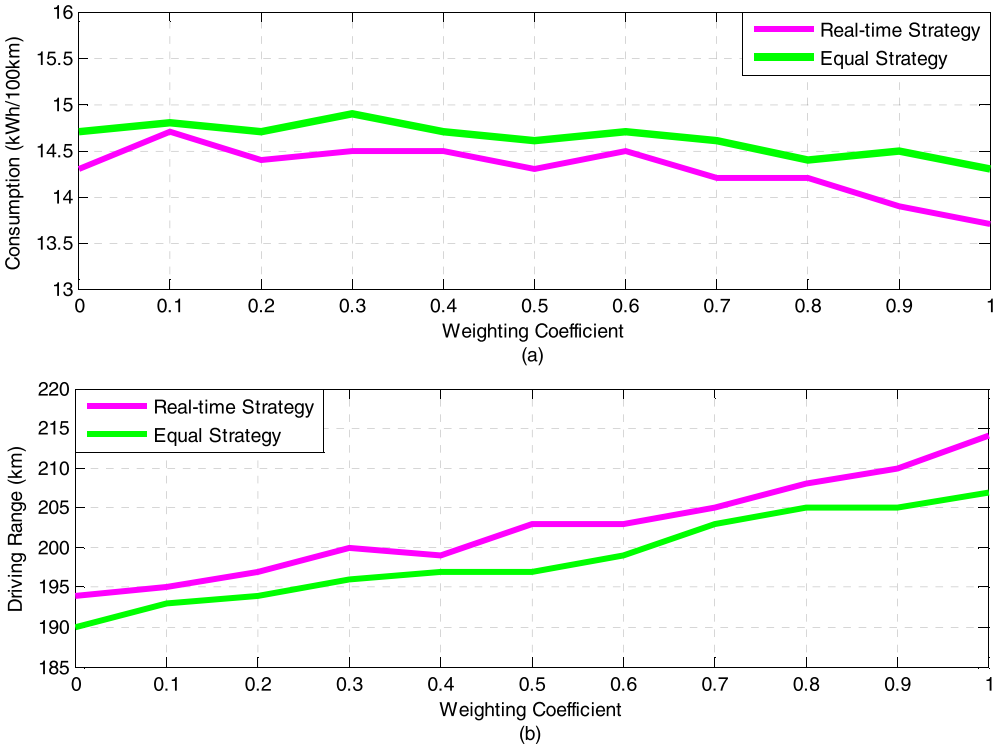

FIGURE 9. Vehicle performance under different torque distribution strategies. (a) Energy consumption for 100 kilometers; (b) Driving range.

TABLE 2. PSO parameters.

Option	Description [a]
Maximum Iterations	400
Number of Particles	40
Inertia	0.9
Global Increment	0.9
Particle Increment	0.9
Maximum Velocity	0.1
Max Failed Runs	5
Failed Run Penalty Value	1.0E30
Failed Run Objective Value	1.0E30

respectively; Ω denotes the feasible solution space; λ_1 and λ_2 are the coefficients to balance the weights of the two optimization objectives; ω_1 and ω_2 are the adjustment coefficients that serve to reduce the value range difference of the two optimization objectives.

D. PARTICLE SWARM OPTIMIZATION ALGORITHM

The PSO is an evolutionary optimization algorithm firstly presented by James Kennedy and Russell C. Eberhart [29] based on the movement and intelligence of the swarms. Mathematically, the PSO method [30], [31] can be described as follows: Each particle has an adaptive value that is determined by the objective function, and the PSO maintains a memory set $\mathrm{P}=\{\mathrm{P}_1, \mathrm{P}_2, \cdots \mathrm{P}_\mathrm{N}\}^\mathrm{T}$, where P_i is the best position ever visited by the i-th particle. In addition, as the PSO allows particles to mutually communicate their experiences, the best position ever visited by all particles can be shared. We define g as the index of the global best position in P, and the global best position is accordingly defined as P_g. At each iteration step t, the particle velocity and position are updated successively according to its own experience as well as the experience of other particles [32]. This process can be described by

$$\begin{aligned} v_i^{t+1} &= v_i^t + \alpha r_1(P_i^t - x_i^t) + \beta r_2(P_g - x_i^t) \\ x_i^{t+1} &= x_i^t + v_i^{t+1} \end{aligned} \tag{37}$$

where r_1 and r_2 are two uniformly random numbers independently distributed in the interval [0, 1], and are used to maintain the diversity of the swarm. v_i and x_i are the velocity and the assigned position of each particle; α and β are the cognitive and the social parameters (or acceleration parameters), which drives particles towards local and global best positions. The flowchart of the PSO algorithm is illustrated in Figure 6.

IV. SIMULATION RESULTS AND DISCUSSION

In this section, we firstly discuss the energy consumption under the proposed distribution strategy and the equal distribution strategy. Then, the parameter optimization results and vehicle performance under two kinds of torque distribution strategies are discussed. As described in Eq. (36), the

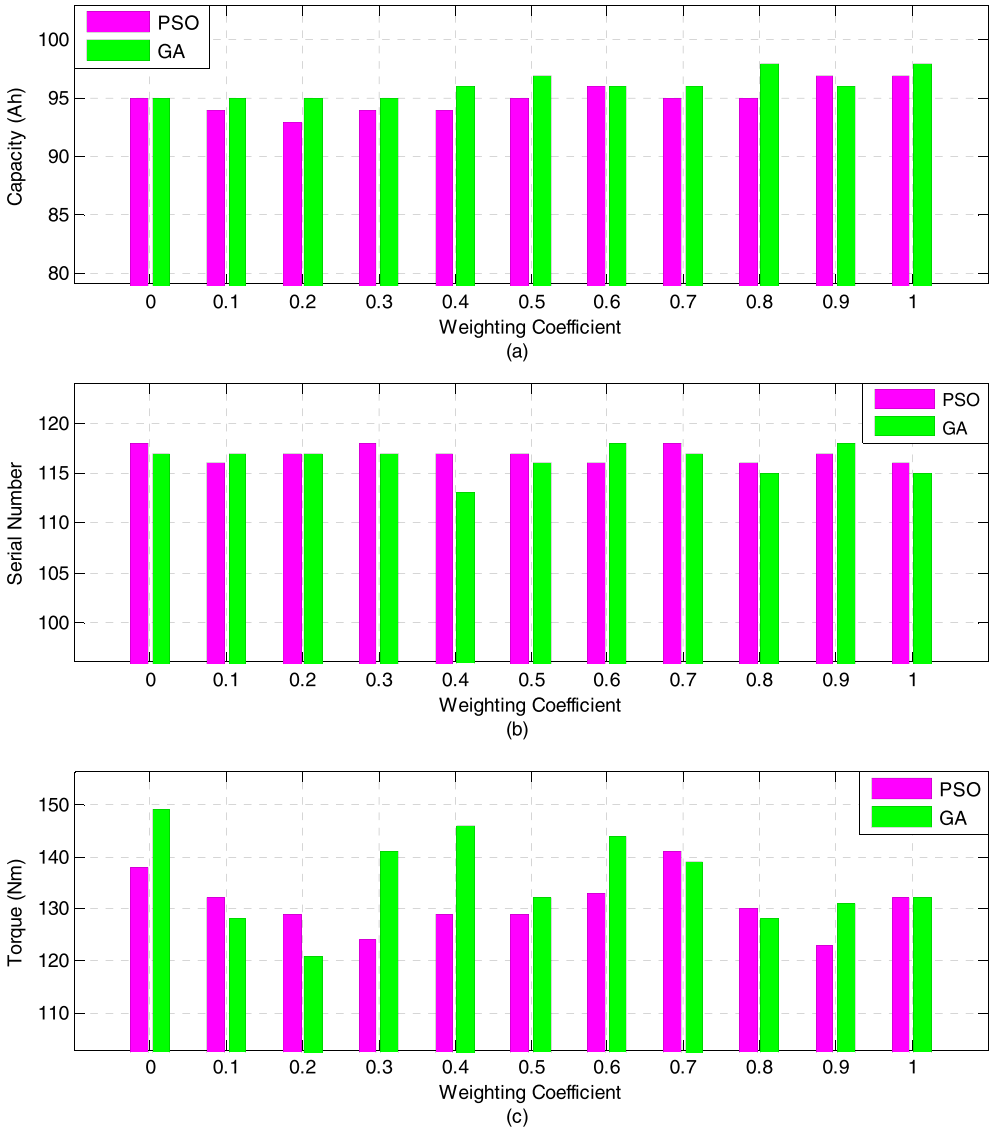

FIGURE 10. The selection of vehicle parameters for PSO and GA algorithm.

coefficients λ_1 and λ_2 are used to balance the weights of the driving range per charge and the energy consumption per hundred kilometers.

It is worth noting that the proposed algorithm was coded in MATLAB, and simulations were conducted on a E5-2630@2.6GHz Intel Xeon V2 processer with 32GB random access memory (RAM). The task of optimizing each mechanical design problems was carried out by using 25 independent runs [33], [34].

A. OPTIMAL TORQUE DISTRIBUTION OF THE FWIA

The real-time distribution strategy for the front-axle and rear-axle motors considering the efficiency of in-wheel motors was proposed to increase the overall efficiency. A complex driving simulation was performed to evaluate its validity. Here, a test based on the New European Driving Cycle (NEDC) was employed to compare the real-time torque distribution strategy with the equal distribution strategy.

Figure 7(a) shows the vehicle velocity in the NEDC driving cycle.

Figure 7(b) and (c) show that the driving torques from the front-axle and rear-axle motors under the two torque distribution strategies. The first one is the equal distribution strategy, which means the driving torques generated from the front-axle and rear-axle motors are always identical. The second one is the proposed optimal real-time distribution strategy, in which discrepant torques are dispatched to the front-axle and rear-axle motors. On occasions that require high accelerations, such as the time periods of 11-14s, 206-209s and 401-404s, larger torque allocation is placed on the front-axle motors to fulfill the power demand with consideration of the overall motor efficiency.

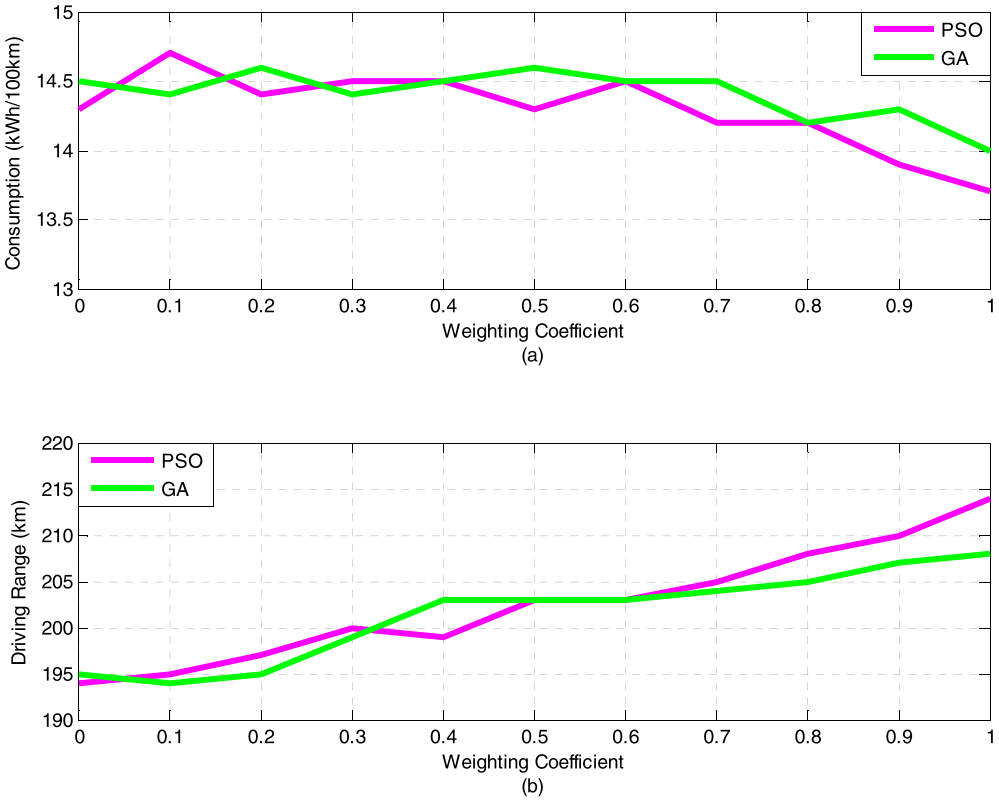

FIGURE 11. The weight coefficient of the PSO and GA algorithm; (a) The driving range and (b) The driving range per kilowatt hour.

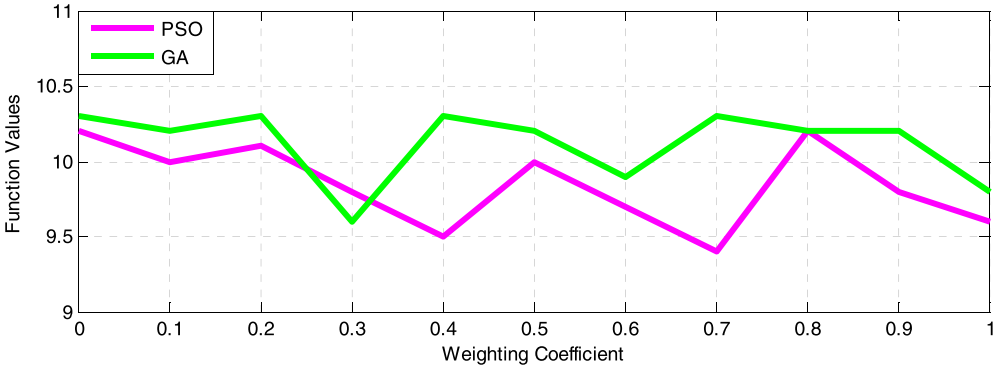

FIGURE 12. Function Value of PSO and GA algorithm.

Figure 7(d) and (e) depict the variation of the efficiencies in the front-axle and rear-axle motors with the two torque distribution strategies.

For the front-axle motors, it can be seen that the frequency of using low-torque area becomes lower in the low-efficiency area under high acceleration scenarios. However, the front-axle motors do not often work under the real-time torque distribution strategy. For the rear-axle motors, it can also be seen that the motor efficiency increases when the real-time torque distribution strategy is applied, and the motor efficiency is improved compared with that under the equal distribution strategy. This can be attributed to the fact that both efficiencies of the front-axle and rear-axle motors are considered when distributing torques, which allows to reasonably expect an improved overall powertrain efficiency.

Figure 7(f) presents the relationship between the SOC values to the driving range per charge, and the simulation results reveal that the driving range per charge can be improved by about 7.8% under the NEDC cycle.

B. POWERTRAIN COMPONENT SIZING OPTIMIZATION

As shown in Figure 8, in order to further examine the effects of the real-time torque distribution strategy and the equal distribution strategy, a series of component optimization

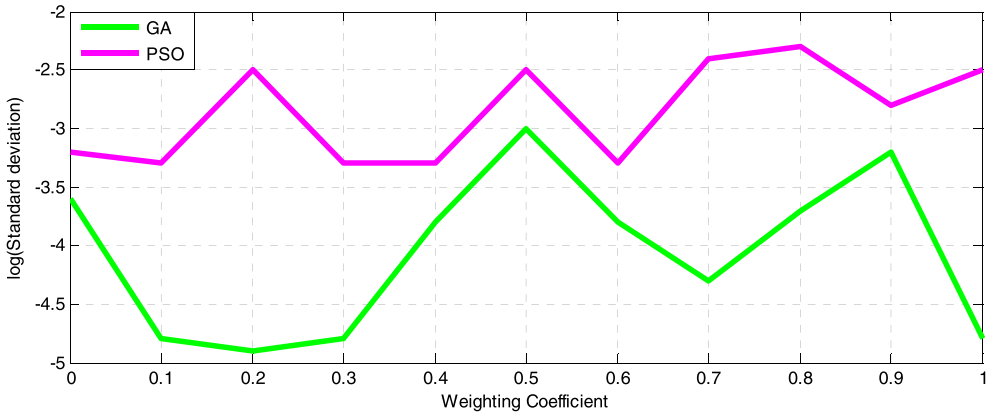

FIGURE 13. The standard deviation of function value for PSO and GA algorithm.

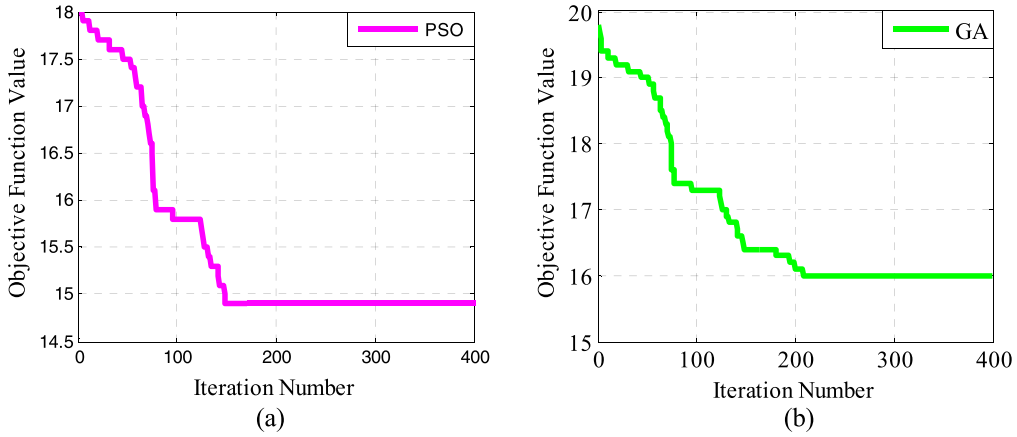

FIGURE 14. Convergence of two algorithms for PSO and GA (a) PSO; (b) GA.

experiments based on the PSO algorithm were conducted in a wide range of λ_1. Figure 8(a)-(d) compare the capacity, battery serial number, and rated motor speed and torque with the presented strategies. As shown in the figures, the vehicle performance with the real-time torque distribution strategy is better than that with the equal distribution strategy under all different weighting coefficients. Especially, the battery cell capacity under the equal distribution strategy increases considerably in comparison with that under the real-time torque distribution strategy, and the maximum increase can reach as high as 4%. The battery number under the equal distribution strategy is also larger than that under the real-time torque distribution strategy, and the maximum increase reaches about 2%. This validates that both battery cell capacity and battery number can be effectively reduced without compromising the vehicle performance under the real-time torque distribution strategy. The rated torque and speed of the selected motors under the equal distribution strategy increase 12% and 9% in contrast to the selection under the real-time torque distribution strategy, respectively. This also verifies that lighter and smaller motors can be used under the real-time torque distribution strategy. In all, it can be reasonably concluded that the component sizing under the real-time distribution strategy is better than that with the equal distribution strategy, which verifies the superiority of the proposed real-time torque distribution strategy.

The driving range per charge and the energy consumption per hundred kilometers are also evaluated and compared under the two torque distribution strategies as shown in Figure 9. It can be seen that the real-time torque distribution strategy outperforms its counterpart on both criteria. The proposed real-time torque distribution strategy can effectively enhance the overall powertrain efficiency through optimizing the operating points of motors. As such, smaller sizing of battery packs and motors can be realized, which would further contribute to vehicle weight reduction and driving range extension.

C. COMPREHENSIVE ANALYSIS OF THE COMPONENT SIZING

In the component sizing optimization, the main parameters of the PSO algorithm need to be defined suitably in advance. According to the value variation ranges of optimization parameters presented in several existing papers and some

primary tests, the values of these parameters adopted in this study are listed in Table II.

In order to verify the optimization results [35]–[38], the GA was also utilized to search for the optimal sizing. As shown in Figure 10, the difference between the optimization results is quite small so that the mutual verification can be reasonably claimed. However, regarding to the two concerned criteria, the optimization results based on the PSO is generally better than that based on the GA as indicated in Figure 11. This is also manifested by the objective function values achieved by the two optimization methods as depicted in Figure 12 and Figure 13. It is clear that the objective values under distinct weight coefficients based on the PSO are smaller and more robust as implied by the smaller standard deviation. Furthermore, the PSO exhibits faster convergence as illustrated in Figure 14. Thus, it is reasonable to conclude that the proposed PSO-based optimization procedure for optimal sizing of an FWIA EV is effective and outperforms the state-of-art GA algorithm.

V. CONCLUSIONS

In this paper, the particle swarm optimization method (PSO) is presented to realize the optimal component sizing of a FWIA electric vehicle. A real-time optimal torque distribution method was also developed and used with the aim to simultaneously increase the driving range per change and reduce the specific energy consumption. To this end, the characteristics of the main components and their key influencing factors were analyzed. Compared with the equal torque distribution strategy, the proposed real-time optimal torque distribution strategy can substantially increase the driving range while reducing the power consumption, which considerably benefits for the vehicle weight reduction and component downsizing. Finally, the PSO-based component sizing, combined with the real-time torque distribution strategy, was proved effective through simulation, and exhibited better performance than the state-of-art GA-based optimization, regarding to optimization results, robustness, and convergence time.

APPENDIX

Nomenclature

m	vehicle mass
m_{bat}	battery mass
m_{motor}	motor mass
Q_0	battery rated capacity
q_{batt}	mass specific energy of the battery
P_{cyc_d}	the battery output power under driving state
P_{cyc_c}	the battery output power under braking state
v(t)	vehicle velocity
η_t	mechanical efficiency of transmission system
η_m	efficiency of motors and motor controllers
η_{ac}	the proportion of energy consumption for accessories
T_{cyc}	the driving time of single driving cycle
ω_{cyc}	motor rotary speed under certain driving cycle
R	the internal resistance of the battery
m_{box}	battery box mass
m_r	the rest of the components mass
U_0	the battery rated voltage
N	the number of batteries
T_{max}	the maximum torque of motor
η_{b_d}	discharge efficiency of battery
η_{b_c}	charge efficiency of battery
ω_N	motor rated rotary speed
ω_{max}	maximum rotary speed
T_N	rated power of motor
$Tmax$	maximum power of motor
ξ_{SOC}	discharge depth
U_{OC}	the voltage of the battery
$P_{b\max}$	battery maximum power

REFERENCES

[1] L. Zhang, X. Hu, Z. Wang, F. Sun, and D. Dorrell, "A review of supercapacitor modeling, estimation, and applications: A control/management perspective," *Renew. Sustain. Energy Rev.*, vol. 81, no. 2, pp. 1868–1878, Jan. 2018.

[2] Z. Wang, J. Ma, and L. Zhang, "Finite element thermal model and simulation for a cylindrical Li-ion battery," *IEEE Access*, vol. 5, pp. 15372–15379, Jul. 2017.

[3] D. Kim, S. Hwang, and H. Kim, "Vehicle stability enhancement of four-wheel-drive hybrid electric vehicle using rear motor control," *IEEE Trans. Veh. Technol.*, vol. 57, no. 2, pp. 727–735, Mar. 2008.

[4] R. Wang and J. Wang, "Fault-tolerant control for electric ground vehicles with independently-actuated in-wheel motors," *J. Dyn. Syst. Meas. Control*, vol. 134, no. 2, pp. 194–203, Jan. 2012.

[5] R. Wang and J. Wang, "Fault-tolerant control with active fault diagnosis for four-wheel independently driven electric ground vehicles," *IEEE Trans. Veh. Technol.*, vol. 60, no. 9, pp. 4276–4287, Nov. 2011.

[6] Y. Chen, X. Li, C. Wiet, and J. Wang, "Energy management and driving strategy for in-wheel motor electric ground vehicles with terrain profile preview," *IEEE Trans Ind. Informat.*, vol. 10, no. 3, pp. 1938–1947, Aug. 2014.

[7] S. Murata, "Innovation by in-wheel-motor drive unit," *Vehicle Syst. Dyn.*, vol. 50, no. 6, pp. 807–830, Jun. 2012.

[8] S. Harada and H. Fujimoto, "Range extension control system for electric vehicles during acceleration and deceleration based on front and rear driving-braking force distribution considering slip ratio and motor loss," in *Proc. 39th Annu. Conf. Ind. Electron. Soc.*, Vienna, Austria, Nov. 2013, pp. 6626–6631.

[9] Y. Wang, H. Fujimoto, and S. Hara, "Torque distribution-based range extension control system for longitudinal motion of electric vehicles by LTI modeling with generalized frequency variable," *IEEE/ASME Trans. Mechatronics*, vol. 21, no. 1, pp. 443–452, Feb. 2015.

[10] H. Fujimoto and S. Harada, "Model-based range extension control system for electric vehicles with front and rear drivingŰbraking force distributions," *IEEE Trans. Ind. Electron.*, vol. 62, no. 5, pp. 3245–3254, May 2015.

[11] J. Park, H. Jeong, I. G. Jang, and S. H. Hwang, "Torque distribution algorithm for an independently driven electric vehicle using a fuzzy control method," *Energies*, vol. 8, no. 8, pp. 8537–8561, Aug. 2015.

[12] J. Kim, "Optimal power distribution of front and rear motors for minimizing energy consumption of 4-wheel-drive electric vehicles," *Int. J. Automot. Technol.*, vol. 17, no. 2, pp. 319–326, Apr. 2016.

[13] R. Wang, Y. Chen, D. Feng, X. Huang, and J. Wang, "Development and performance characterization of an electric ground vehicle with independently actuated in-wheel motors," *J. Power Sources*, vol. 196, no. 8, pp. 3962–3971, 2011.

[14] H. Lee, D. Tesar, and P. Ashok, "Expanded human choice based on duty/demand cycles for in-wheel motors in electric vehicles," *SAE Int. J. Passenger Cars-Mech. Syst.*, vol. 10, no. 1, pp. 1–12, Mar. 2017.

[15] Y. Chen and J. Wang, "Adaptive energy-efficient control allocation for planar motion control of over-actuated electric ground vehicles," *IEEE Trans. Control Syst. Technol.*, vol. 22, no. 4, pp. 1362–1373, Apr. 2014.
[16] J. Wu, C.-H. Zhang, and N.-X. Cui, "PSO algorithm-based parameter optimization for HEV powertrain and its control strategy," *Int. J. Automot. Technol.*, vol. 9, no. 1, pp. 53–59, Feb. 2008.
[17] H. Sun, L. Yang, and J. Jing, "Hydraulic/electric synergy system (HESS) design for heavy hybrid vehicles," *Energy*, vol. 35, no. 12, pp. 5328–5335, Dec. 2010.
[18] X. Yuan and J. Wang, "Torque distribution strategy for a front- and rear-wheel-driven electric vehicle," *IEEE Trans. Veh. Technol.*, vol. 61, no. 8, pp. 3365–3374, Oct. 2012.
[19] Z. Dimitrova and F. Maréchal, "Techno-economic design of hybrid electric vehicles using multi objective optimization techniques," *Energy*, vol. 91, pp. 630–644, Nov. 2015.
[20] L. Li, Y. Zhang, C. Yang, X. Jiao, L. Zhang, and J. Song, "Hybrid genetic algorithm-based optimization of powertrain and control parameters of plug-in hybrid electric bus," *J. Franklin Inst.*, vol. 352, no. 3, pp. 776–801, Mar. 2015.
[21] Z. Chen, N. Guo, X. Li, J. Shen, R. Xiao, and S. Li, "Battery pack grouping and capacity improvement for electric vehicles based on a genetic algorithm," *Energies*, vol. 10, no. 4, p. 439, Mar. 2017.
[22] J. Soares, T. Sousa, H. Morais, Z. Vale, B. Canizes, and A. Silva, "Application-specific modified particle swarm optimization for energy resource scheduling considering vehicle-to-grid," *Appl. Soft Comput.*, vol. 13, no. 11, pp. 4264–4280, 2013.
[23] S. Ganguly, "Multi-objective planning for reactive power compensation of radial distribution networks with unified power quality conditioner allocation using particle swarm optimization," *IEEE Trans. Power Syst.*, vol. 29, no. 4, pp. 1801–1810, Jul. 2014.
[24] L. Xu, C. D. Mueller, J. Li, M. Ouyang, and Z. Hu, "Multi-objective component sizing based on optimal energy management strategy of fuel cell electric vehicles," *Appl. Energy.*, vol. 157, pp. 664–674, Nov. 2015.
[25] M. Daneshyari and G. G. Yen, "Constrained multiple-swarm particle swarm optimization within a cultural framework," *IEEE Trans. Syst., Man, Cybern. A, Syst. Humans*, vol. 42, no. 2, pp. 475–490, Mar. 2012.
[26] L. Zhang, Z. Wang, X. Hu, F. Sun, J. Deng, and D. Dorrell, "Multi-objective optimal sizing of hybrid energy storage system for electric vehicles," *IEEE Trans. Veh. Technol.*, to be published, doi: 10.1109/TVT.2017.2762368.
[27] Y. Tang, E. Motoasca, J. J. H. Paulides, and E. A. Lomonova, "Comparison of flux-switching machines and permanent magnet synchronous machines in an in-wheel traction application," *COMPEL-Int. J. Comput. Math. Elect. Electron. Eng.*, vol. 32, no. 1, pp. 153–165, Jan. 2013.
[28] M. Abdul-Hak, N. Al-Holou, and U. Mohammad, "Predictive intelligent battery management system to enhance the performance of electric vehicle," in *Electric Vehicles—Modelling and Simulations*. Rijeka, Croatia: InTech. [Online]. Available: https://www.intechopen.com/books/howtoreference/electric-vehicles-modelling-and-simulations/predictive-intelligent-battery-management-system-to-enhance-the-performance-of-electric-vehicle
[29] Y. Zhang, S. Wang, and G. Ji, "A comprehensive survey on particle swarm optimization algorithm and its applications," *Math. Problems Eng.*, vol. 2015, Feb. 2015, Art. no. 931256.
[30] A. R. Yildiz, "A novel particle swarm optimization approach for product design and manufacturing," *Int. J. Adv. Manuf. Technol.*, vol. 40, no. 5, pp. 617–628, Jan. 2009.
[31] A. R. Yildiz, "A new hybrid particle swarm optimization approach for structural design optimization in the automotive industry," *Proc. Inst. Mech. Eng., D, J. Automobile Eng.*, vol. 38, no. 11, pp. 1287–1296, Mar. 2012.
[32] M. Dadgar, S. Jafari, and A. Hamzeh, "A PSO-based multi-robot cooperation method for target searching in unknown environments," *Neuro Comput.*, vol. 177, pp. 62–74, Feb. 2016.
[33] A. Ghanei, E. Assareh, M. Biglari, A. Ghanbarzadeh, and A. R. Noghrehabadi, "Thermal-economic multi-objective optimization of shell and tube heat exchanger using particle swarm optimization (PSO)," *Heat Mass Transf.*, vol. 50, no. 10, pp. 1375–1384, Mar. 2014.
[34] N. B. Guedria, "Improved accelerated PSO algorithm for mechanical engineering optimization problems," *Appl. Soft Comput.*, vol. 40, pp. 455–467, Mar. 2016.
[35] A. R. Yildiz, "Comparison of evolutionary-based optimization algorithms for structural design optimization," *Eng. Appl. Artif. Intell.*, vol. 26, no. 1, pp. 327–333, Jan. 2013.
[36] A. R. Yildiz, "A comparative study of population-based optimization algorithms for turning operations," *Inf. Sci.*, vol. 210, no. 1, pp. 81–88, Nov. 2012.
[37] M. Kiani and A. R. Yildiz, "A comparative study of non-traditional methods for vehicle crashworthiness and NVH optimization," *Arch. Comput. Method Eng.*, vol. 23, no. 4, pp. 723–734, Dec. 2016.
[38] A. R. Yildiz, N. Pholdee, and S. Bureerat, "Hybrid real-code population-based incremental learning and differential evolution for many-objective optimisation of an automotive floor-frame," *Int. J. Vehicle Des.*, vol. 73, nos. 1–3, pp. 20–53, Mar. 2017.

ZHENPO WANG received the Ph.D. degree in automotive engineering from the Beijing Institute of Technology, Beijing, China, in 2005.

He is currently a Professor with the Beijing Institute of Technology, where he is also the Associate Director of the Collaborative Innovation Center for Electric Vehicles in Beijing and the National Engineering Laboratory for Electric Vehicles. He has published four monographs, translated books, and over 60 technical papers. He holds over ten patents. His current research interests include pure electric vehicle integration, the packaging and energy management of battery system, and charging station design. He was a recipient of numerous awards, including the Second National Prize for Progress in Science and Technology the First Prize for Progress in Science and Technology from the Ministry of Education, China, and the Second Prize for Progress in Science and Technology from the Beijing Municipal, China.

CHANGHUI QU received the B.S. degree in vehicle engineering from Northeastern University, China, in 2013. He is currently pursuing the Ph.D. degree in mechanical engineering with the National Engineering Laboratory for Electric Vehicles, Beijing Institute of Technology, China. His current research interests include the design and control of the four-wheel independently actuated electric vehicle.

LEI ZHANG (S'12–M'16) received the Ph.D. degree in mechanical engineering from the Beijing Institute of Technology, Beijing, China, in 2016. He is currently an Assistance Professor with the School of Mechanical Engineering, Beijing Institute of Technology.

His research interests include ultracapacitor and battery modeling and state estimation, energy management development for hybrid energy storage system for electric vehicle application, and advanced control in vehicular dynamics.

XUE XUE received the B.S. degree in automotive engineering from the Beijing Institute of Technology, Beijing, China, in 2017. Her current research interests include control of the four-wheel independently actuated electric vehicle and vehicle tests.

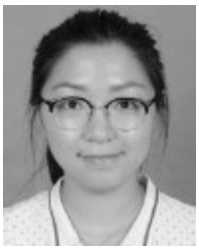

JIANYANG WU received the B.S. degree in detection technology and automatic equipment from the Beijing University of Civil Engineering and Architecture in 2016. She is currently pursuing the Ph.D. degree in mechanical engineering with the National Engineering Laboratory for Electric Vehicles, Beijing Institute of Technology, China. Her research interests include estimation and control systems for four-wheel independently actuated electric vehicles.